1-2022

Experimental Study of Wall Bounded Harbor Seal Whisker Inspired Pin Geometries

Anish Prasad
Embry-Riddle Aeronautical University, prasada3@my.erau.edu

Mark Ricklick
Embry-Riddle Aeronautical University, ridlickm@erau.edu

Experimental Study of Wall Bounded Harbor Seal Whisker Inspired Pin Geometries

Anish Prasad[1] and Mark Ricklick[2]
Embry-Riddle Aeronautical University, Daytona Beach, FL, 32114, USA

Conventional cylindrical/elliptical pins are one of the most widely used geometries in convection cooling systems and are used in the internal cooling of gas turbine blades and other applications, as they promote better heat transfer at the expense of large pressure losses and unsteadiness in the flow. The need to reduce pressure drop and maintain the heat transfer rates are a pressing requirement for a variety of industries to improve their cooling efficiency. One such prominent field of research is conducted in optimizing the design of pin geometries. In this study, a harbor seal whisker inspired geometry is being studied for their unsteady behavior in an internal cooling channel. The seal whisker geometry consists of streamwise and spanwise undulations which reduce the size of the wake and coherent structures shed from the body as a result of an added component of stream-wise vorticity along the pin surface. Also, the vortex shedding frequency becomes less pronounced, leading to significantly reduced lateral loading on the modified cylinder. Previous computational studies have shown that the bio-mimicked pin geometries break down the wake structure and there is a reduction in development of turbulent intensity downstream of the channel leading to a lower pressure loss. In this experimental study the thermal performance of the bio pins is compared against a conventional elliptical pin for a range of Reynolds numbers. From the results it is found that the bio pins in comparison to the elliptical pin performs on average 13% better in pressure drop at the cost of 4.5% in heat transfer. These findings are important to the gas turbine community as reduced penalties associated with cooling flows directly translate to improved efficiencies.

I. Nomenclature

G2TV	=	Bio inspired pin with two valleys
G2TRV	=	Bio inspired pin with three valleys
G2E	=	Elliptical pin
Nu	=	Nusselt number
f	=	Friction factor
Re	=	Reynolds number
X	=	Streamwise direction (m)
Y	=	Spanwise direction (m)
D, D_h	=	Characteristic diameter (m)
H	=	Height (m)
CFD	=	Computational Fluid Dynamics
TSP	=	Temperature Sensitive Paint
VARIAC	=	Variable Alternating Current Transformer
CMOS	=	Complementary Metal Oxide Semiconductor
T	=	Temperature (K)
I	=	Intensity
ΔT	=	Temperature difference (K)
k	=	Thermal conductivity (W/m.K)
q	=	Heat supplied (W)
q"	=	Heat flux (W/m^2)
$\dot{m}$	=	Mass flow rate (kg/S)
C_p	=	Specific heat (J/Kg.K)
Subscripts		
0	=	Smooth channel case
s	=	Surface
ref	=	Reference
sup	=	Supplied

II. Introduction

Most energy-based systems in-use employ some form of convection based thermal management. Most of the passenger aircrafts operating today are powered by gas turbine engines. The efficiency of the gas turbine is directly related to the turbine inlet temperature, and the effectiveness of the hot section cooling systems. Modern gas turbine

[1] Ph.D. Student, Aerospace Engineering Department, Embry-Riddle Aeronautical University.
[2] Assistant Professor, Aerospace Engineering Department, Embry-Riddle Aeronautical University.

designs have taken advantage of advanced cooling technologies to the extent that rotor inlet temperatures several hundred Kelvin beyond the melting point of the exotic materials used within them have been achieved [1], with limits continuing to be pushed. The importance of this is highlighted by the fact that a 56 Kelvin increase in hot gas temperature potentially yields an increase of up to 13% in power output or 4% in simple cycle efficiency [2]. Future advances, however, are becoming more difficult to achieve, as the rate of technology improvement has somewhat reached a plateau in the past 10 years [3,4]. There is a need in improved cooling techniques which take the advantage of advanced materials and their manufacturing methods. In most heat exchange applications, an array of constant cross section cylinders are widely employed; hence they have been heavily studied in the literature.

The circular cross section cylinders have higher heat transfer characteristics at the cost of pumping power requirements in comparison to other conventional pins, hence increasing heat transfer characteristics will subsequently increase the pumping power requirements. It has been found that the behavior of flow around the pin impacts the heat transfer and it's also been found that the presence of the pin breaks up the boundary layer creating a horseshoe vortex. This horseshoe vortex produces high wall shear stress beneath it, resulting in high heat transfer from the wall in this region [5]. The resulting flow separation around the pin, however, results in large pressure losses. The pin fin channel has been heavily studied in the literature [6-10], in an effort to describe the heat transfer and flow behavior and improve prediction abilities. The circular cylindrical pins are relatively easy to manufacture and hence, this configuration is often found in commercial applications. However, the advent of advanced manufacturing techniques has brought about focus in uniquely shaped pins in an effort to improve the effectiveness of these configurations.

Several researchers have investigated benefits associated with non-conventional pins. For example, Kim and Moon [11] investigated a stepped circular pin shape, in an effort to enhance heat transfer and thermal performance. They showed that significant improvements were possible as compared to straight pin shapes. Tullius [12] investigated the impact of normal, non-circular fin shapes on heat transfer in a microchannel, with improved performance observed with triangular pins. Pent [13] investigated the performance of a porous pin fin array, in an attempt to reduce the pressure drop across the system. However, the size of the wake was increased along with pressure penalties. Uzol and Camci [14] conducted a study to compare end-wall heat transfer enhancements and total pressure loss between circular, elliptical and a pin based on NACA 0024 airfoil. The circular pin outperformed the other two shapes thermally while the latter showed significant pressure loss reduction. Optimization techniques have also been carried out by several other groups as well [15, 16].

Biomimicry and bio-inspired devices have gained interest recently, due to the optimized designs presented in nature through evolution. It is a new discipline that imitates natural designs to solve problems [17]. Biomimicry has found applications in a variety of fields, including modeling bumblebees and other insects in flapping wing aerodynamics [18, 19], gas sampling based on canine olfactory airflows [20], as well as in the industrial design sector [21]. Performance gains and technological insight have been seen in all sectors.

The harbor seal whisker has been studied heavily in the literature, in an effort to understand their acute sensing abilities [22, 23]. The undulated shape of the whiskers results in reduced vortex excitations and smaller organized flow structures behind the whisker [24-27]. This leads to reduced lifting forces and flow induced vibrations, making them an ideal solution to micro-sensors [28-33]. NASA researchers have investigated the benefits associated with larger scale structures, such as adaptations to turbine blades [34], and other structures [35]. Reduced aerodynamic loading and total pressure losses have been observed, associated with the streamwise vortex-mainstream flow interactions. In general, the elimination of large-scale coherent structures and resulting reduced wake size have an all-around positive impact aerodynamically. With the advent of advanced manufacturing techniques, such as three-dimensional printing of high strength alloys [36], implementation of such devices is now a possibility.

Previous studies involved computational work with bio-mimicked pin geometries, these geometries did not retain the same structural pattern as the harbor seal whiskers, and these computational results were later compared experimentally [37, 38]. The results of those studies show an agreement for using computational tool for performing more studies on this topic. Computational studies were performed for pins which retain the same structural pattern as the whiskers, Fast Fourier Transform (FFT) on these pins have shown that the harbor seal whisker pin geometries breakdown the wake structure which contributes to the reduction in pressure drop, as the turbulence mixing in the downstream of the channel decreases in intensity [39]. The current study intends to compare the thermal performance of the bio pins with a conventional elliptical pin in pin fin channel experimental setup for a range of Reynolds numbers.

III. Pin Model

The harbor seal whiskers have two distinct elliptical shapes, one at the peak and one at the valley, as seen in Fig. 1. The bio pin created in this study are scaled uniformly 12.6 times from the whiskers natural dimensions [27]. The dimensions of the pins made in this study: period of the undulations is 11.466 mm, peak major and minor radius are

7.497 mm and 3.024 mm, valley major and minor radius are 5.985 mm and 3.654 mm, and the peak and valley plane angle are 15.27° and 17.60°. The height of the pins for this study is 30 mm.

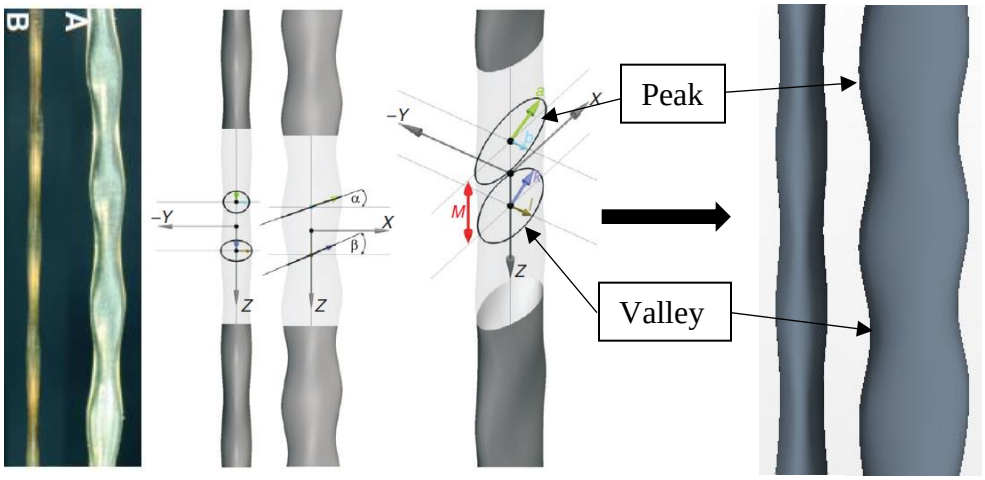

Fig. 1 Seal whisker structure [27]

The pin geometry for this study is made by cropping the bio pins to retain two valley, and one peak (G2TV) and three valley, and two peaks (G2TRV). The conventional elliptical pin (G2E) is based on the minor and major diameter of the valley of the bio pin. The endwall blockage for the channel is the same for all the pin design used. The pins are 3D printed using a third-party 3D printing service (Shapeways) as seen in Fig. 2. Most of the 3D printed pins are made of versatile plastic (Nylon 12), few pins are made of aluminum alloy (AlSi10Mg).

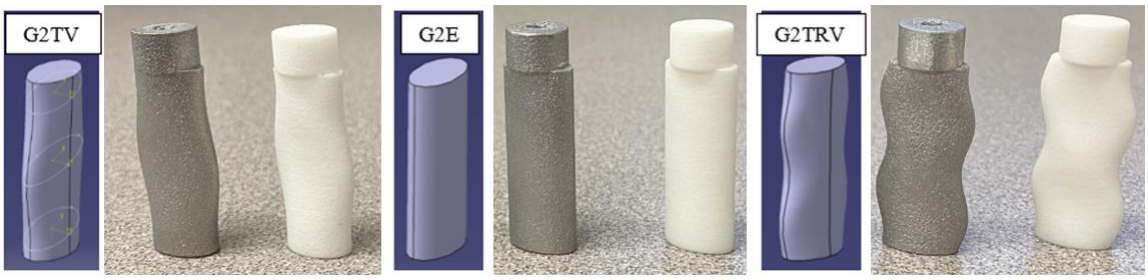

Fig. 2 Pin Geometry

IV. Experimental Setup

A pin fin channel was created using acrylic plates for the experimental study as shown in Fig. 3. The pin array in the test section was composed of 8 rows of pins, 7 pins in each row, arranged in a staggered manner with spanwise (Y) and streamwise (X) spacing of 45 mm each and channel height (H) of 30 mm. The exit section was connected to the suction side of the blower using pipes. The air flow was controlled using valves. The mass flow is calculated using the difference in pressure measured using a venturimeter. The velocity is calculated based on the mass flow and the inlet area of the test section test section, hence the calculated velocity will be the inlet velocity of the test section. Reynolds number is based on the inlet velocity and the characteristic length scale (2H). Reynolds number of 15,000, 30,000, 60,000 and 85,000 is used in this study.

The end wall of the acrylic test section was painted with a uniform coat of Temperature Sensitive Paint, above which the strips were placed using a double sided high-strength tape. The strips were connected in series using copper bus bars. These were then connected to a VARIAC to form a series circuit. The pins were placed on top of the Inconel heater strips. Some of the pins were internally heated using cartridge heaters specifically the central section of the setup to reduce lateral conduction. The data from the regions surrounding these pins are post-processed and presented in this paper. A scientific grade CMOS camera was used to capture the TSP, which was excited by LED light of particular as shown in Fig. 3. A constant heat flux was supplied to the Inconel strips through Joule heating by varying the voltage.

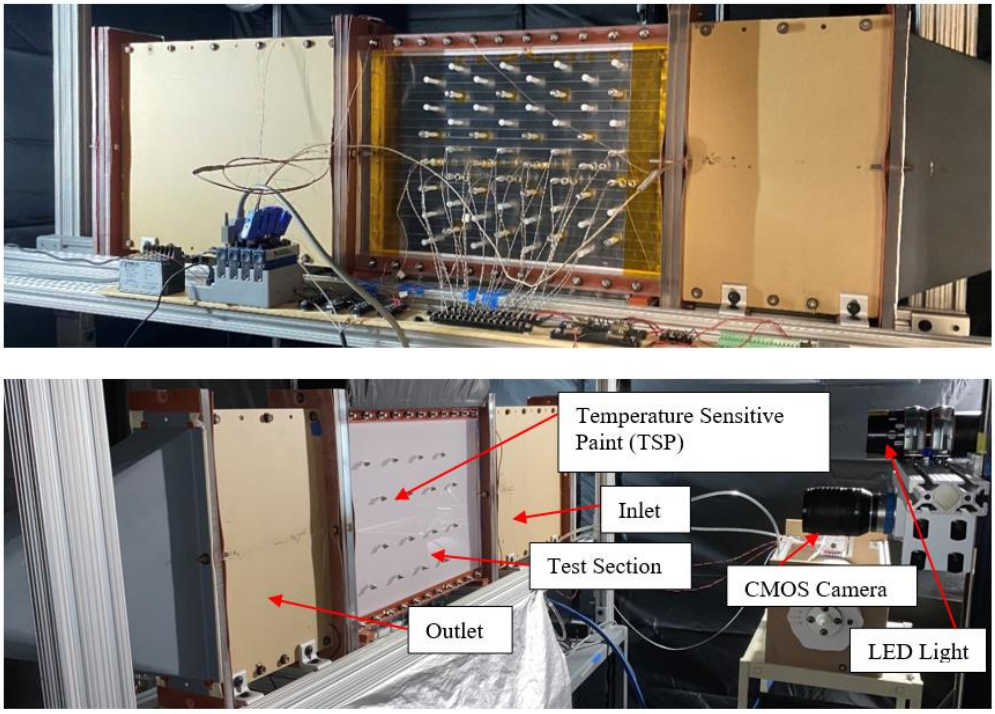

Fig. 3 Setup and view of test section.

As seen from Fig. 3 sixteen fasteners are used to secure a proper fit between the top and bottom plate, since acrylic plates warp due to constant heating, which leads to the pins not touching the bottom plate. Hence this problem is avoided by using fasteners. The schematic of the test section is shown in Fig. 4.

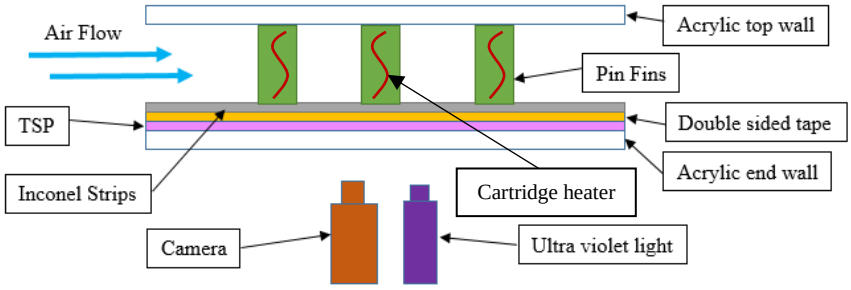

Fig. 4 Schematic of the wall and test section

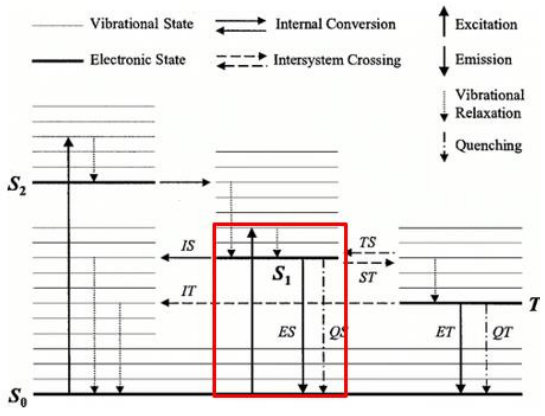

Fig. 5 Jablonski diagram [42]

TSP provides a convenient way to obtain local temperature data. It is a luminescent paint with fluorescent molecules suspended within a binder. The TSP molecules are excited to a higher energy state when exposed to light of appropriate wavelength (excitation wavelength). Jablonski diagram shown in Fig. 5, describes the transition of the molecules. They can return to ground state by emitting photons of particular wavelength (emission wavelength) through luminescence and without emitting photons by thermal quenching. In thermal quenching the molecules vibrate and collide with one another, losses energy and returns to ground state.

In a given instant the molecules return to the ground state by both luminescence and thermal quenching, but the number of molecules returned by each method differs

statistically in regard to temperature applied. For this research ISSI brand UniCoat TSP [40] was used having excitation wavelength of 380 – 520 nm and emission wavelength of 500 – 720 nm. An ultraviolet light with a wavelength of 460 nm (from manufacturer ISSI [41]) was used to excite the TSP molecules. The intensity of the paint varies with the number of photons emitted. Increase in temperature will statistically increase the return of photons to ground state through thermal quenching, thereby decreasing the intensity of the paint (intensity is related to the measure of photons emitted from the TSP, which are then captured by the photodetector).

Fig. 6 Reference Image & Data Image

In Fig. 6, the reference image is taken before the heated run with known intensity and reference temperature (measured and confirmed with multiple thermocouples across different locations). The data image is that of the heated run where the intensity of the paint is known but the surface temperature of the paint is unknown.

TSP is calibrated with a calibration curve of intensity ratio vs temperature difference. Using this calibration curve, the temperature of the data image can be found. The calibration uncertainty of TSP was found to be ± 0.93 °C for temperature ranges of 22 to 90 °C in previous studies[43]. A scientific grade camera (CMOS) is used to capture the intensity of the light emitted by the TSP, with a long pass filter (wavelength 550 nm) to distinguish between the excited and the emitted wavelength. A detailed description of TSP and PSP technologies has been presented by Liu [43], Sullivan [44].

V. Endwall Data Reduction

The calibration curve for the TSP is given by,

$$\frac{T_S - T_{ref}}{100} = 2.52\left(\frac{I_S}{I_{ref}}\right)^4 - 8.30\left(\frac{I_S}{I_{ref}}\right)^3 + 10.18\left(\frac{I_S}{I_{ref}}\right)^2 - 6.24\left(\frac{I_S}{I_{ref}}\right) + 1.85 \quad (1)$$

A constant heat flux was supplied to the Inconel strips. In order to account for the heat lost to the surrounding through the channel endwall, a heat leakage test was conducted. The test section was filled with insulating material to prevent natural convection, and a heat flux was applied to the bottom wall. The applied heat flux under these conditions was assumed to pass through the acrylic wall into the room. The heat lost to surrounding was found at several wall temperatures, and correlated as a function of the difference in temperature between the wall and room, given by,

$$q''_{loss} = 6.3144 * \Delta T \quad (2)$$

The bulk temperature is calculated as,

$$T_{bk}^{i(x)} = T_{bk}^{i-1(x)} + \frac{q(x)}{\dot{m}C_p} \quad (3)$$

The left-hand side of the equation is the bulk temperature of the current pixel in the *x* direction (streamwise) calculated using the bulk temperature of the previous pixel. *q(x)* is the heat supplied per pixel, ṁ is the mass flow rate into the channel while C_p is the specific heat capacity of the air based on the mean bulk temperature.

The Nusselt number was calculated using the following equation:

$$Nu = \frac{\frac{q''_{sup} - q''_{loss}}{(T_s - T_{bk})} * D}{k} \quad (4)$$

VI. Results

A smooth channel test was done in order to establish confidence in the results obtained from our test setup and measurement techniques before progressing further. The spanwise averaged Nusselt number for smooth channel was compared with Gnielinski correlation [45] as shown in equation 5.

$$Nu_D = \frac{(f/8)(Re_D - 1000)Pr}{1 + 12.7(f/8)^{1/2}(Pr^{2/3} - 1)} \tag{5}$$

Where f is the friction factor which is calculated using Darcy–Weisbach equation, as shown in equation 6. This correlation is valid for $0.5 < Pr < 2000$ and $3000 < Re_D < 5 \times 10^6$. Figure 7 shows the spanwise average Nusselt number for the smooth channel test for the Reynolds number case of 60,000.

$$f = \frac{2 * \Delta P * D_h}{L * \rho * v^2} \tag{6}$$

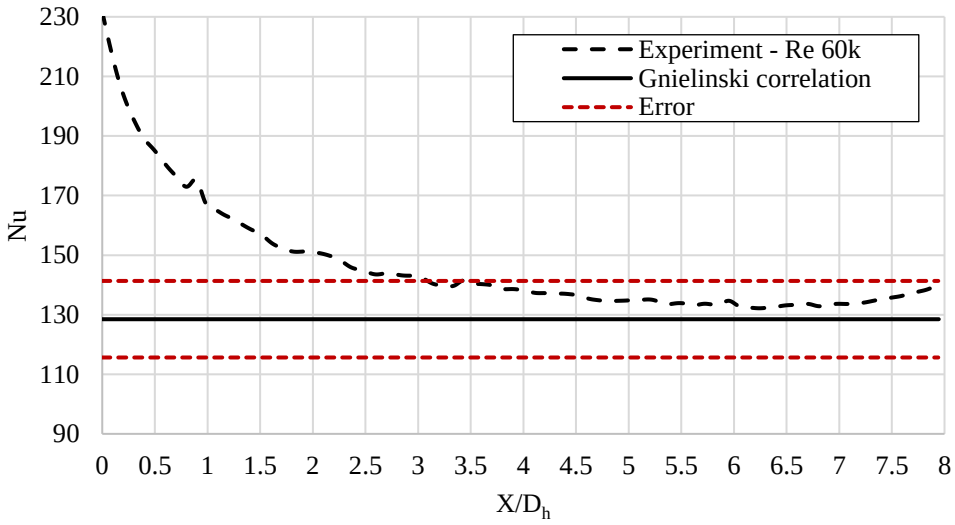

Fig. 7 Spanwise Average Smooth Channel Nusselt Number

Since heating begins at the start of the test section, the impact of thermal development of the flow is seen up to approximately at an X/D_h of 4. After this point we can say that the flow becomes fully thermally developed. Comparing the result to the correlation we can see that the spanwise average is in good agreement, well within 10% of given uncertainty. Figure 8 shows the post processed image of TSP for the smooth channel test for Reynolds number of 30,000.

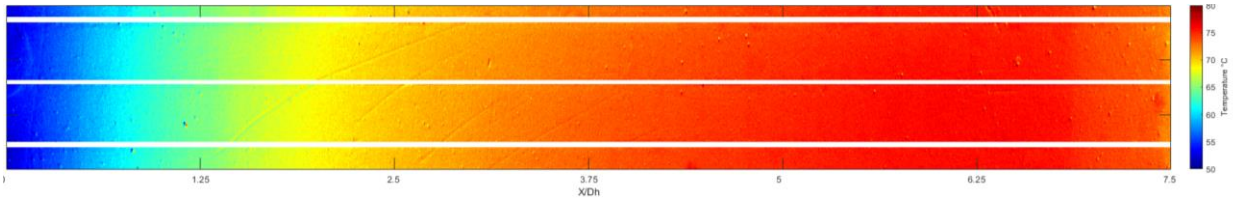

Fig. 8 Temperature Contour

Figure 9 shows the end wall Nusselt number contour for Re of 30,000. From the figure we can see that behind row 1 the wake region is much narrower for pin G2TRV in comparison to the other pins, this trend can be seen almost behind every row for G2TRV. Looking at the data downstream of the channel we can see that pin G2E has an increase in magnitude of heat transfer compared to other two pins.

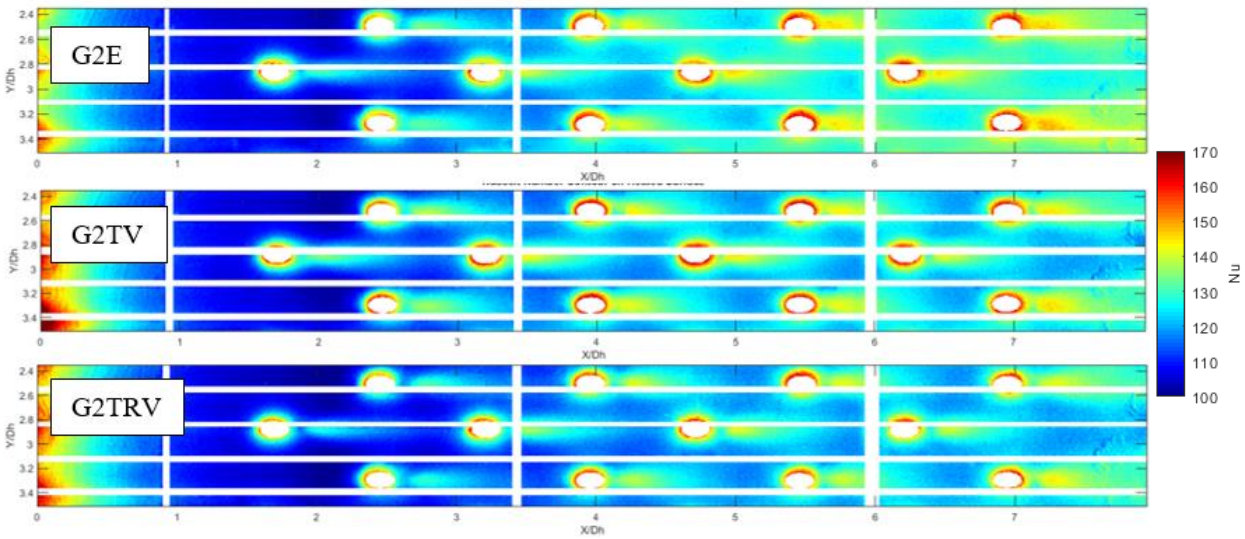

Fig. 9 Nusselt number contour for Re = 30,000

The uncertainty in this experimental study is calculated using the Root Sum Square Method [46, 47]. Figure 10 shows the Nusselt number variation across different Reynolds number. From this result, it can be seen that the difference between the heat transfer performance is maintained between 1 – 2%. With G2E being the best performer followed by G2TV and G2TRV. The uncertainty in the results is approx. 9.4% for Reynolds number case of 15,000 and 30,000 and approx. 8.5% for Reynolds number case of 60,000 and 85,000. The uncertainty in the Reynolds numbers is approx. 2.8%.

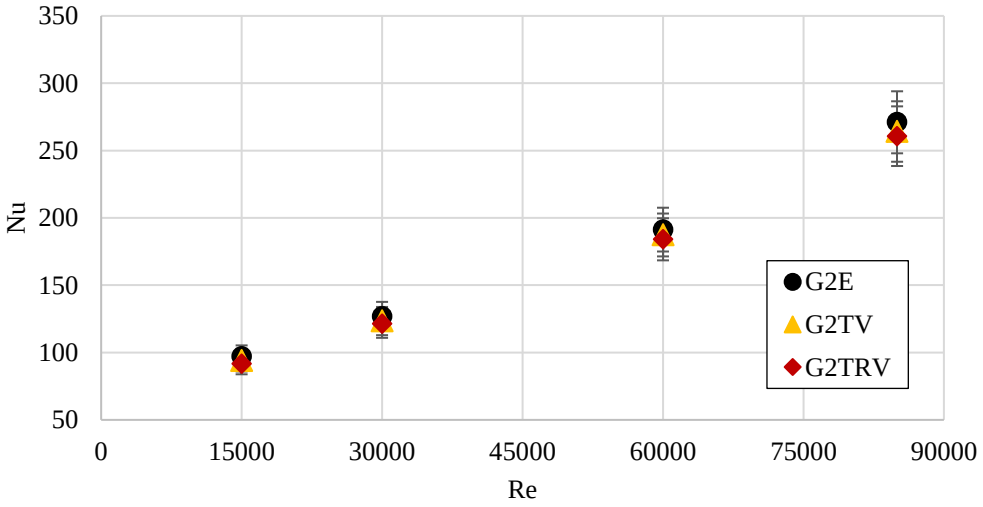

Fig. 10 Endwall Nusselt number over Reynolds number

Figure 11 – Figure 14 shows the endwall Nusselt number vs friction factor. The endwall average Nusselt number is normalized with respect to the smooth channel results and compared with the friction factor normalized with smooth channel friction factor for respective Reynolds number. The friction factor is calculated using Darcy-Weishbach equation as shown in equation 6. The uncertainty in the results is approx. 10% for normalized Nusselt number and approx. 5% for normalized friction factor for Reynolds number of 15,000. For Reynolds number of 30,000 its 11.5% and 3.3%, for 60,000 its 8.5% and 3% and for 85,000 its 9.5% and 2.7%.

As seen from the results, in comparison to pin G2E, the bio pins G2TV and G2TRV performs 9.84% - 16.11% better in pressure drop at a cost of 3.54% - 5.59% in heat transfer for the Reynolds number case of 15,000.

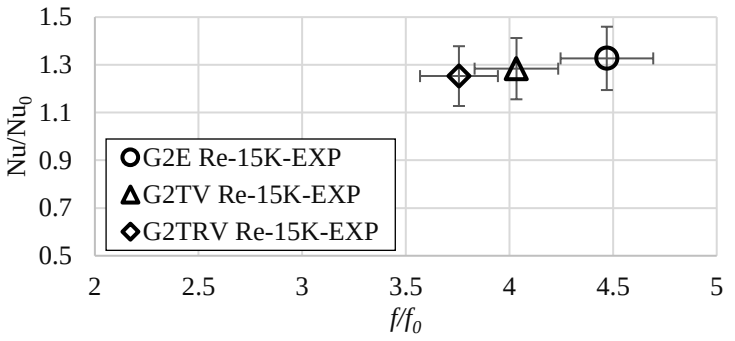

Fig. 11 Normalized Nu vs f for Re = 15,000

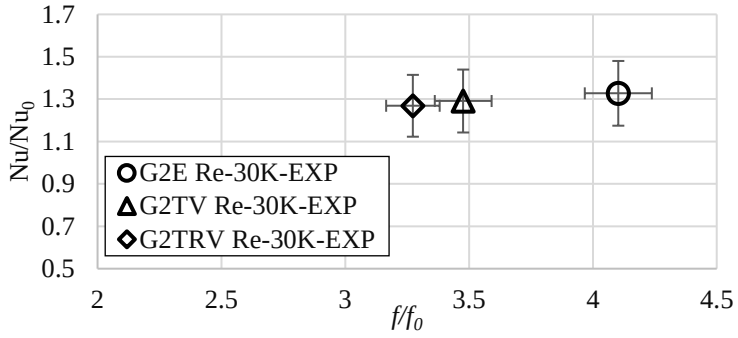

Fig. 12 Normalized Nu vs f for Re = 30,000

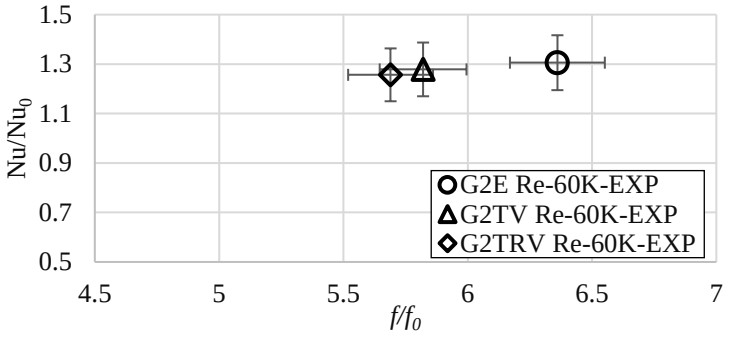

Fig. 13 Normalized Nu vs f for Re = 60,000

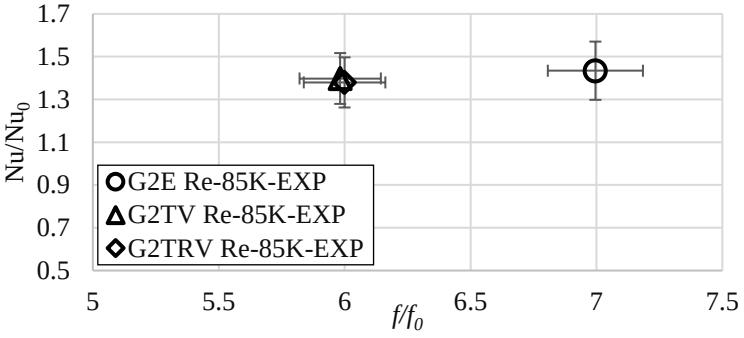

Fig. 14 Normalized Nu vs f for Re = 85,000

Similar observation could be made for other Reynolds number cases. One notable difference is that for a high Reynolds number of 85,000 the thermal performance of G2TV and G2TRV are the same. And the difference in heat transfer between G2E and the bio bins decreases from 5.5% to 3.5% as the Reynolds number is increased, with an overall improvement in friction factor performance by 14%. The behavior of the pins shown in these results could be seen in the pressure drop and spanwise surface average Nusselt number results.

Figure 15 – Figure 18 shows the pressure drop data for Reynolds number case of 15000, 30000, 60000 and 85000. The pressure data are obtained from the side wall in the test section. Each port is located between two rows of pins, first port is located before the first row and the last port is located after the last row. The pressure drop across the channel is calculated based on the difference between the first port and the subsequent port. The experimental uncertainty is calculated to be 7%, 5.5%, 4% and 3.3% for Reynolds number case of 15000, 30000, 60000 and 85000.

From the figures we can see that the bio pin has reduced pressure drop in the channel in comparison to the elliptical pin. This is due to pin G2E having periodic wake shedding which leads to an increase in flow mixing downstream of the channel contributing to large pressure drop. Whereas the bio pins have a reduction in the wake magnitude and flow mixing leading to decrease in pressure drop along the channel.

From these results we can see that as the Reynolds number is increased the magnitude difference between the static pressure loss for pin G2TV and G2TRV decreases, this is due to fact that as the momentum in the flow is increased the magnitude of flow mixing downstream of the channel is increased as well, leading to loss of uniqueness of the pin wake structure.

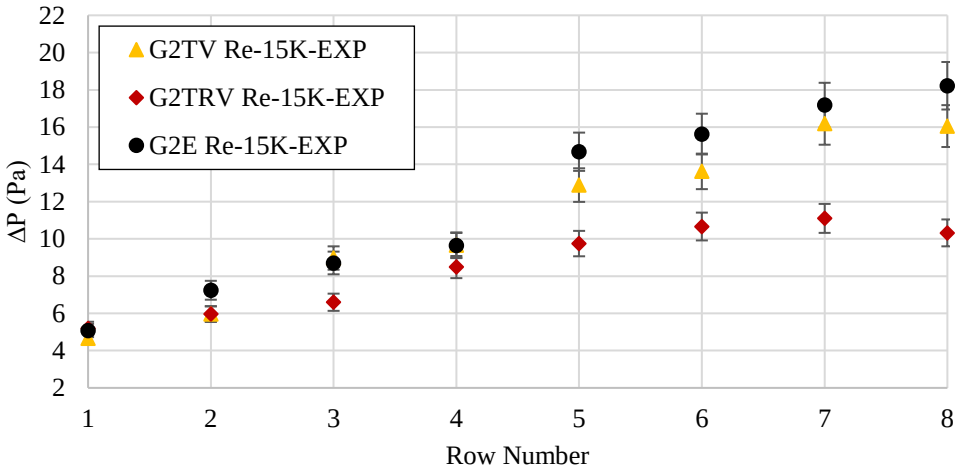

Fig. 15 Pressure drop along the channel – Re = 15,000

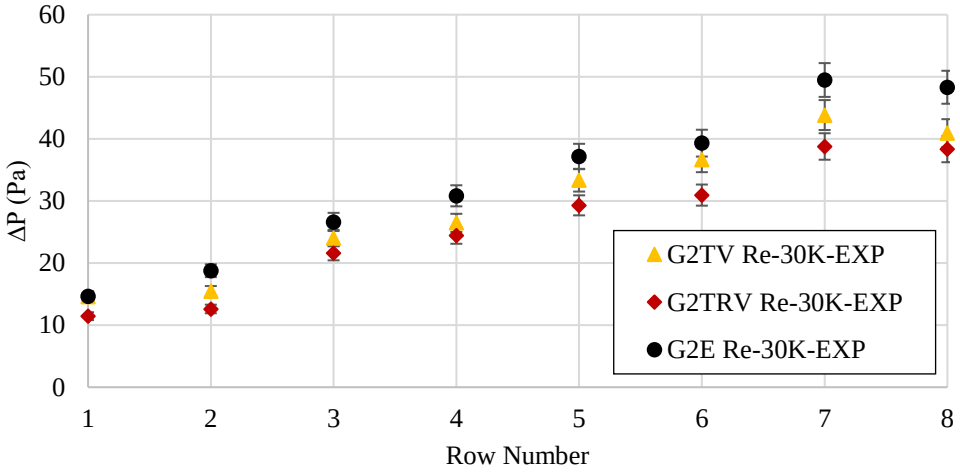

Fig. 16 Pressure drop along the channel – Re = 30,000

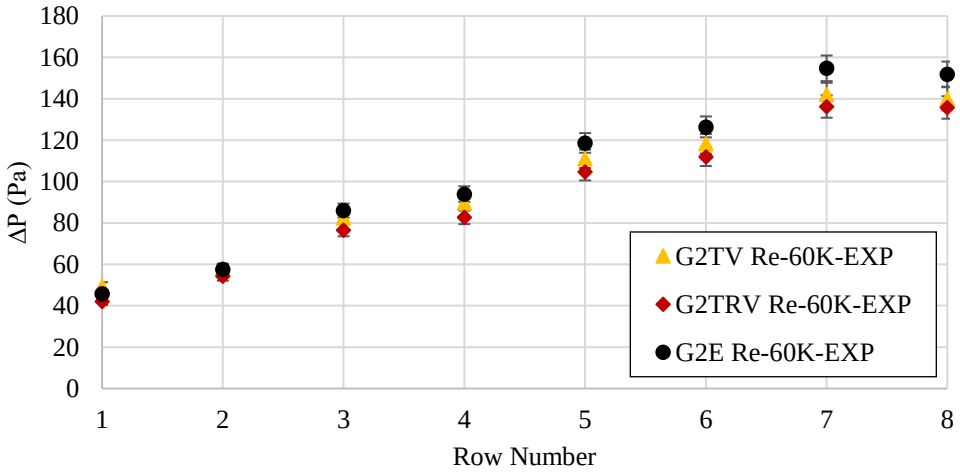

Fig. 17 Pressure drop along the channel – Re = 60,000

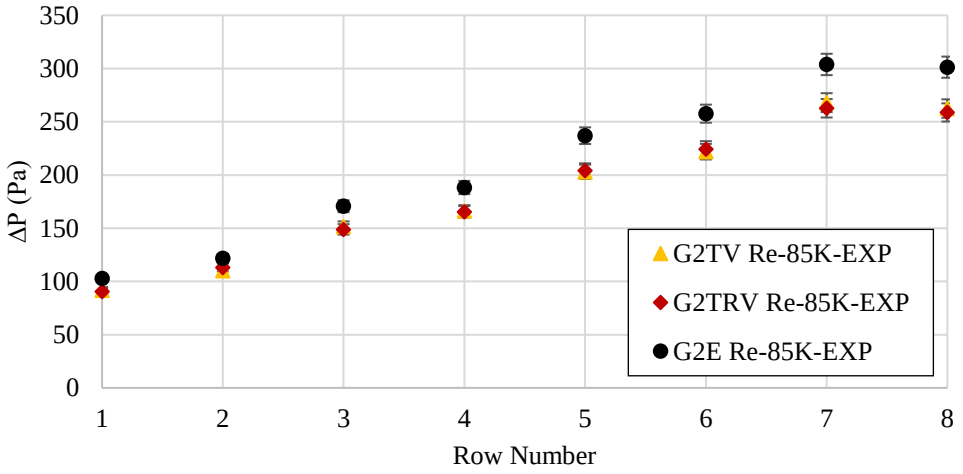

Fig. 18 Pressure drop along the channel – Re = 85,000

To study the spanwise data the spanwise average Nusselt number was normalized with respect to square root of Reynolds number to obtain Frossling number. Figure 19 – Figure 22 represents the spanwise average Frossling number along the streamwise direction for all four Reynolds numbers. From the spanwise results, we can see that as the Reynolds number is increased the difference between the spanwise average Frossling number for pin G2TV and G2TRV decreases after Row 3. This is due to fact that as the momentum in the flow is increased the magnitude of flow mixing downstream of the channel is increased as well, leading to loss of uniqueness of the pin wake structure.

On comparing between the bio pins and pin G2E, we can see that the pin G2E still has a better heat transfer augmentation downstream of the channel. This is due to G2E having periodic wake shedding which leads to an increase in turbulence fluctuations at the endwall as the flow moves through the channel. The bio pins G2TV and G2TRV having reduced wake size due to the presence of the undulation leads to a reduction in magnitude of flow mixing downstream of the channel thereby leading to the decrease in endwall Nusselt number.

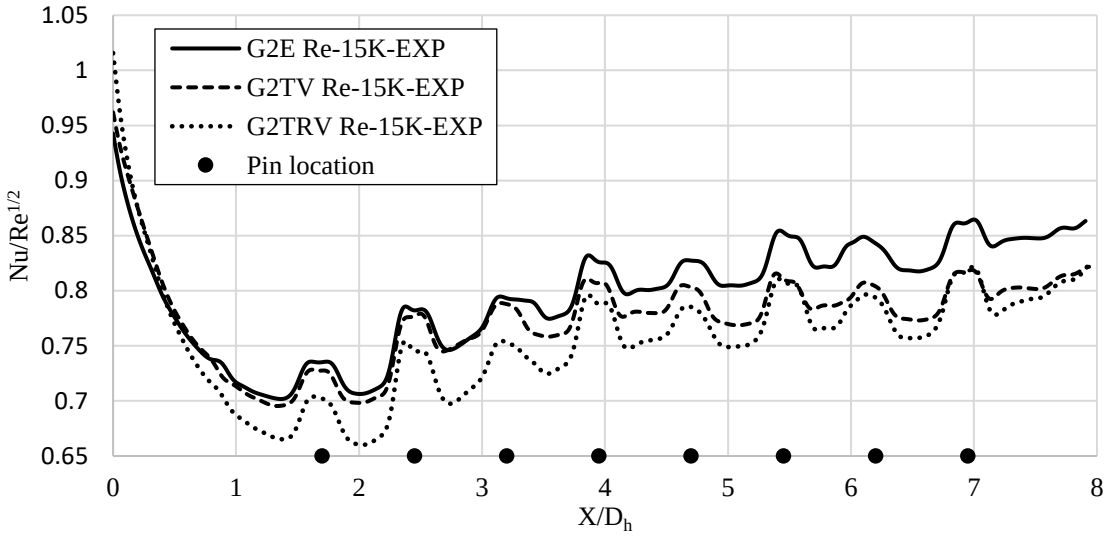

Fig. 19 Spanwise averaged Nusselt number for Re = 15,000

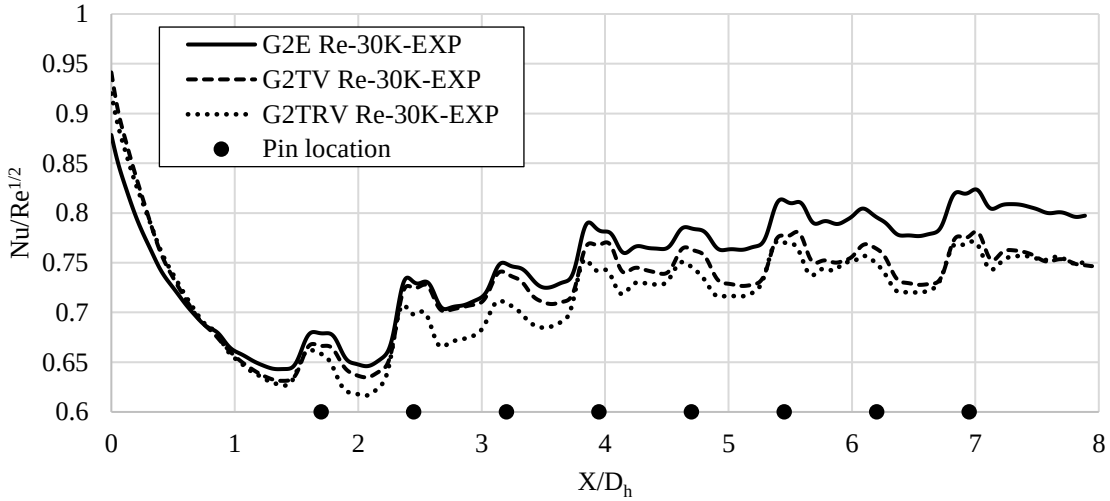

Fig. 20 Spanwise average Nusselt number for Re = 30,000

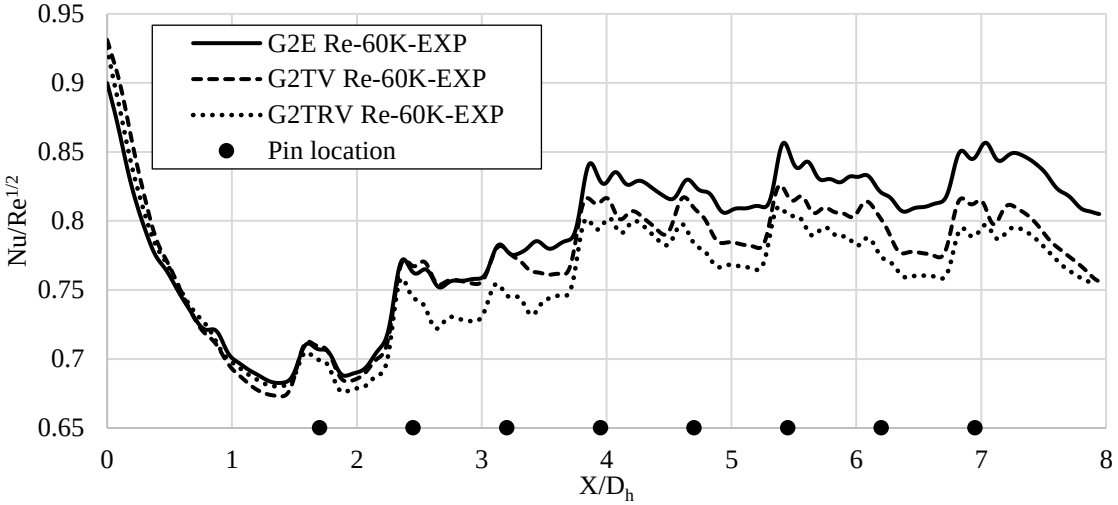

Fig. 21 Spanwise average Nusselt number for Re = 60,000

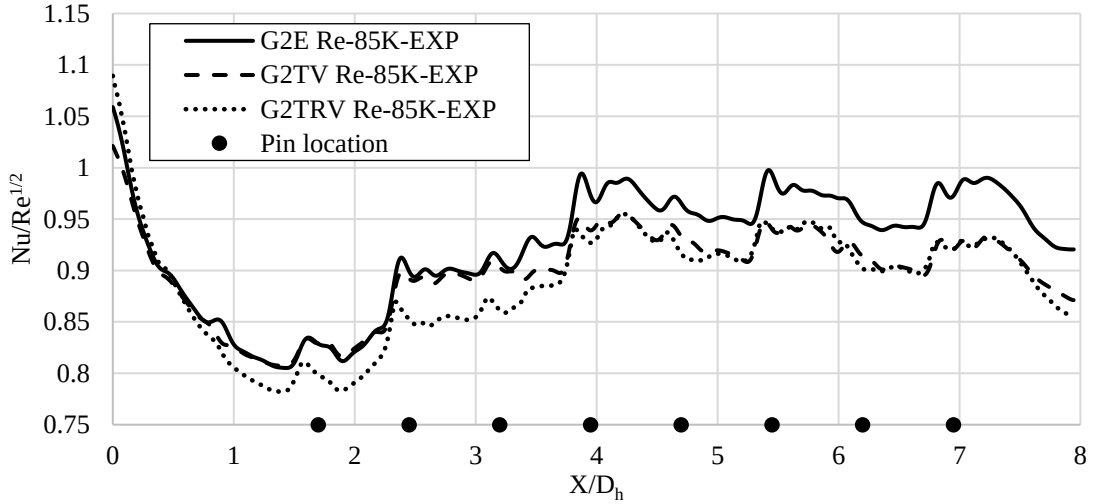

Fig. 22 Spanwise average Nusselt number for Re = 85,000

VII. Conclusion

The objective of this study was to experimentally investigate the thermal performance of harbor seal whisker inspired pin geometries in a pin-fin channel. From the result discussed above it is understood that the harbor seal whisker pin geometries breakdown the wake structure which contributes to the reduction in pressure drop, as the turbulence mixing in the downstream of the channel decreases in intensity. This reduction in pressure drop reduces the Nusselt number which is related to reduced turbulence mixing. Table 1 compares the thermal performance at constant pressure drop and at constant pumping power for pins G2E, G2TV and G2TRV for all four Reynolds numbers. Results in column 3 shows thermal performance at constant pressure drop and column 4 shows thermal performance at constant pumping power.

Table. 1 Summary

Re	Case	$\frac{\frac{Nu}{Nu_0}}{\frac{f}{f_0}}$	$\frac{\frac{Nu}{Nu_0}}{\left(\frac{f}{f_0}\right)^{1/3}}$
15,000	G2E	0.296	0.098
	G2TV	0.318	0.106
	G2TRV	0.333	0.111
30,000	G2E	0.323	0.107
	G2TV	0.371	0.123
	G2TRV	0.387	0.129
60,000	G2E	0.205	0.068
	G2TV	0.219	0.073
	G2TRV	0.221	0.076
85,000	G2E	0.205	0.068
	G2TV	0.233	0.077
	G2TRV	0.229	0.076

The thermal performance data is normalized with respect to smooth channel data, hence a higher value indicates better performance. From the results we can see that the bio pins perform better in comparison to elliptical pin G2E in terms of thermal performance at constant pressure drop and pumping power, with a maximum difference of 11% and 13% for the lower Reynolds number case. As the harbor seal whisker is elliptical in nature pin G2E was used as a comparison instead of a conventional cylindrical pin. It can be seen from this study that the pin geometries inspired from harbor seal whiskers do have the potential to improve thermal performance.

Furthermore, the impact of endwall heat transfer and pressure drop in the channel are related to the magnitude of wake created by the pins, flow acceleration and turbulence mixing in the channel. Hence other engineered pin designs can be implemented such as, helical strake on a circular cylinder. Helical strakes are used in cylindrical towers to minimize flow induced vibrations by reducing the wake size generated by these towers. Numerous studies have been carried out on pin shapes, such as oblong pins, teardrop shaped pins, NACA airfoil shaped pins, triangular pins and so on. This shows that there are other engineering designs and also other potential nature designs available to be implemented in a pinfin channel configuration for thermal management purpose, with harbor seal whisker pin designs being one more potential solution.

References

[1] Sautner, M., Clouser, S., and Han, J.C., "Determination of Surface Heat Transfer and Film Cooling Effectiveness in Unsteady Wake Flow Conditions," *AGARD Conference Proceedings 527*, 1992, pp. 6-1 to 6-12.

[2] Boyce, M.P., *Gas Turbine Engineering Handbook*, Gulf Professional Publishing, 3rd edition, 2006, pp 47-48.

[3] Bunker, Ronald S., "Gas Turbine Heat Transfer: Ten Remaining Hot Gas Path Challenges," *Journal of Turbomachinery*, Vol. 129, 2007, pp. 193-201.
doi: 10.1115/1.2464142

[4] Downs, J.P., and Landis, K.K., "Turbine Cooling Systems Design- Past, Present and Future," *Proceedings of ASME Turbo Expo 2009*, GT2009-59991, 2009.
doi: 10.1115/GT2009-59991

[5] Chyu, M.K., and Goldstein R.J., "Influence of an array of wall-mounted cylinders on the mass transfer from a flat surface," *International journal of heat and mass transfer*, Vol. 34, No. 9, 1991.
doi: 10.1016/0017-9310(91)90044-F
[6] VanFossen, G. J., "Heat Transfer Coefficients for Staggered Arrays of Short Pin Fins" *ASME Journal of Engineering for Power*, Vol. 104, 1982, pp. 268-274.
doi: 10.1115/1.3227275
[7] Chyu, M., Hsing, Y., Shih, T., Natarajan, V., "Heat transfer contributions of pins and endwall in pin-fin arrays: effects of thermal boundary condition modeling," *Journal of Turbomachinery*, Vol. 121, No. 2, 1999, pp. 257-263.
doi: 10.1115/1.2841309
[8] Ames, F.E., and Dvorak, L.A., "Turbulent Transport in Pin Fin Arrays: Experimental Data and Predictions", *Journal of Turbomachinery*, Vol. 128, 2006, pp. 71-81.
doi: 10.1115/1.2098792
[9] Ciha, K. T., "Pressure Loss through Multiple Rows of Various Short Pin Array Geometries & A Survey of Pressure Loss and Heat Transfer through Multiple Rows of Short Pin Arrays", Prepared for Southwest Research Institute, Mechanical Engineering Division, 2014.
[10] Ricklick, M., and Carpenter, C., "Comparison of Heat Transfer Prediction for Various Turbulence Models in a Pin Fin Channel," *50th AIAA Joint Propulsion Conference*, Cleveland, OH, 2014.
doi: 10.2514/6.2014-3838
[11] Kim, K., and Moon, M., "Optimization of a stepped circular pin-fin array to enhance heat transfer performance," *Heat and Mass Transfer*, Vol. 46, 2009, pp. 63-74.
doi: 10.1007/s00231-009-0544-3
[12] Tullius, J., Tullius, T., and Bayazitoglu, Y., "Optimization of short micro pin fins in minichannels," *International Journal of Heat and Mass transfer*, Vol. 55, 2012, pp. 3921-3932.
[13] Pent, J. M., Kapat, J. S., and Ricklick, M., "Comparison of Pressure Drop and End Wall Heat Transfer Measurements to Flow Visualization Testing of Solid and Porous Pin Fin Arrays," *ASME 2009 International Mechanical Engineering Congress and Exposition*, 2009, pp. 2101-2111.
doi: 10.1115/IMECE2009-10271
[14] Uzol, O., and Camci, C., "Heat Transfer, Pressure Loss and Flow Field Measurements Downstream of a Staggered Two-Row Circular and Elliptical Pin Fin Arrays," *Journal of Heat Transfer*, Vol. 127, No. 5, 2005, pp. 458-471.
doi: 10.1115/1.1860563
[15] Kondo, Y., Matsuhima, H., and Komatsu, T., "Optimization of Pin-Fin Heat Sinks for Impingement Cooling of Electronic Packages," *Journal of Electronic Packaging*, Vol. 122, 2000.
doi: 10.1115/1.1289761
[16] Bejan, A., "Constructal T-shaped fins," *International Journal of Heat and Mass Transfer*, 2000.
doi: 10.1016/S0017-9310(99)00283-5
[17] Benyus, J. M., *Biomimicry*, William Morrow, New York, 1997.
[18] DeLuca, A., "Aerodynamic performance and particle image velocimetry of piezo actuated biomimetic manduca sexta engineered wings towards the design and application of a flapping wing flight vehicle," Ph.D. Dissertation, Airforce Institute of Technology, 2013.
[19] Thompson, M., Burnett, J., Batra, A., Ixtabalan, D., Tran, D., Rodriguez, A., and Steele, B., "Experimental Design of a Flapping Wing Micro Air Vehicle through Biomimicry of Bumblebees," *Proceedings of AIAA SciTech 2015*, Orlando, FL, 2015.
doi: 10.2514/6.2015-1454
[20] Settles, G.S., Douglas A.K., and Lori J.D-D., "The external aerodynamics of canine olfaction," *Sensors and sensing in biology and engineering*, Springer Vienna, 2003.
doi: 10.1007/978-3-7091-6025-1_23
[21] Volstad, N., and Boks, C., "On the use of Biomimicry as a Useful Tool for the Industrial Designer," *Sustainable Development*, Vol. 20, No. 3, 2012, pp. 189-199.
doi: 10.1002/sd.1535
[22] Beem, H., and Triantafyllou, M., "Exquisitely sensitive seal whisker-like sensors detect wakes at large distances," *Massachusetts Institute of Technology Library*, 2015.
[23] Miersch, L., Hanke, W., Wieskotten, S., Hanke, T., Oeffner, J., Leder, A., Brede, M., Witte, M., and Dehnhardt, G., "Flow Sensing by Pinniped Whiskers," *Philosophical Transactions of Royal Society B*, 2011.
doi: 10.1098/rstb.2011.0155
[24] Beem, H., Dahl, J., and Triantafyllou, M., "Harbor Seal Vibrissa Morphology Reduces Vortex Induced Vibrations," *64th Annual Meeting of the APS Division of Fluid Dynamics*, 2011.
[25] Weymouth, G., and Triantafyllou, M., "Numerical Study of Seal Whisker Vibrations," *64th Annual Meeting of the APS Division of Fluid Dynamics*, 2011.
[26] Murphy, C. T., Eberhardt, W.C., Calhoun, B.H., Mann, K.A., and Mann, D.A., "Effect of angle on flow-induced vibrations of pinniped vibrissae". *PLoS ONE*, Vol. 8, No.8, 2013.
doi: 10.1371/journal.pone.0069872

[27] Hanke, W., Witte, M., Miersch, L., Brede, M., Oeffner, J., Michael, M., and Hanke, F., "Harbor Seal Vibrissa Morphology Suppresses Vortex Induced Vibrations," *Journal of Experimental Biology*, Vol. 213, 2010, pp. 2665-2672. doi: 10.1242/jeb.043216
[28] Hans, H., Miao J., Weymouth G., and Triantafyllou, M., "Whisker-like geometries and their force reduction properties," *2013 MTS/IEEE Oceans*, Bergen, Norway, 2013. doi: 10.1109/OCEANS-Bergen.2013.6608113
[29] Kottapalli, A., Asadnia, M., Miao, J., and Triantafyllou, M., "Harbor seal whisker inspired flow sensors to reduce vortex-induced vibrations," *28th IEEE International Conference on Micro Electro Mechanical Systems*, Estoril, Portugal, 2015. doi: 10.1109/MEMSYS.2015.7051102
[30] Hans, H., Valdivia P., Thekoodan, D., Jianmin, M., and Triantafyllou, M., "A whisker sensor: role of geometry and boundary conditions," *64th Annual Meeting of the APS Division of Fluid Dynamics*, 2011.
[31] Kottapalli, A., Asadnia, M., Miao, J., and Triantafyllou, M., "Harbor seal whisker inspired flow sensors to reduce vortex-induced vibrations," *28th IEEE International Conference on Micro Electro Mechanical Systems*, Estoril, Portugal, 2015. doi: 10.1109/MEMSYS.2015.7051102
[32] Liu, Y., Tian, L., and Barbastathis, G., "Study of a seal whisker-inspired flow sensor using compressive holography," *Digital Holography and Three-Dimensional Imagining*, Kohala Coast, Hawaii, 2013. doi: 10.1364/DH.2013.DTh4A.5
[33] Beem, H., and Triantafyllou, M., "Seal whisker-inspired circular cylinders reduce vortex-induced vibrations," *APS Division of Fluid Dynamics*, 2012.
[34] Shyam, V., Ameri, A., Poinsatte, P., Thurman, D., Wroblewski, A., and Snyder, C., "Application of Pinniped Vibrissae to Aeropropulsion," *Proceedings of ASME Turbo Expo 2015*, Montreal, Canada. GT2015-43055, 2015. doi: 10.1115/GT2015-43055
[35] Fernandes, R., Ricklick, M., and Pai, Y., "CFD Benchmarking of Heat Transfer and Pressure Drop Predictions in a Pin Fin Channel." *51st AIAA/SAE/ASEE Joint Propulsion conference*, 2015. doi: 10.2514/6.2015-3736
[36] Bernstein, J., Bravato, A., Ealy, B., Ricklick, M., Kapat, J., Mingareev, I., Richardson, M., Meiners, and W., Kelbassa, I., "Fabrication and Analysis of Porous Superalloys for Turbine Componenets Using Laser Additive Manufacturing," *49th AIAA Joint Propulsion Conference*. San Jose, CA, 2013. doi: 10.2514/6.2013-4178
[37] Pai, Y., Prasad, A., Fernandes, R. and Ricklick, M.A., "Preliminary Investigation of Bio-Inspired Cylinders for Improved Thermal Performance of Internal Cooling Channels," *53rd AIAA/SAE/ASEE Joint Propulsion Conference*, 2017, pp. 4977. doi: 10.2514/6.2017-4977
[38] Prasad, A., Pai, Y., Ogbebor-Evans, O. and Ricklick, M.A., "Investigation of Bio-Inspired Pin Geometries for Enhanced Heat Transfer Applications," *2018 Joint Propulsion Conference*, 2018, pp. 4429. doi: 10.2514/6.2018-4429
[39] Prasad, A., and Ricklick, M. A., "Unsteady Behavior of Wall Bounded Harbor Seal Whisker Inspired Pin Geometries," *AIAA Scitech 2020 Forum*, 2020, pp. 0633. doi: 10.2514/6.2020-0633
[40] ISSI, Innovative Scientific Solutions, Temperature Sensitive Paint, http://www.psp-tsp.com/index.php?id=123.
[41] ISSI, Innovative Scientific Solutions, High-intensity light sources, http://www.psp-tsp.com/index.php?id=213.
[42] Bell, James, Schairer, E., Hand, L., Mehta, R., "Surface Preassure Measurements Using Luminescent Coatings", *Journal of Fluid Mechanics*, Vol. 33, 2001, pp 155-206. doi: 10.1146/annurev.fluid.33.1.155
[43] Liu, Quan, Kapat, J., "*Study of Heat Transfer Characteristics of Impinging Air Jet Using Pressure and Temperature Sensitive Luminescent Paint*", UCF Dissertation, May 2006.
[44] Liu, T., Campbell, B., Sullivan, J., "*Accuracy of TSP for heat transfer measurements*", AIAA 95-2042, 1995.
[45] Gnielinski, V., "New equations for heat and mass transfer in turbulent pipe and channel flow," *Int. Chem. Eng.*, Vol. 16, No. 2, 1976, pp. 359-368.
[46] Moffat, R. J., "Describing the Uncertainties in Experimental Results," *Experimental Thermal and Fluid Science*, Vol. 1, No. 1, 1988, pp. 3–17. doi: 10.1016/0894-1777(88)90043-X
[47] Prasad, A., and Ricklick, M. A., "A Detailed Uncertainty Analysis of Heat Transfer Experiments Using Temperature Sensitive Paint," *55th AIAA Aerospace Sciences Meeting*, AIAA Paper 2017-1283, 2017. doi: 10.2514/6.2017-1283